[137] G. Rammes, R. Rupprecht, U. Ferrari, W. Zieglgansberger, C. G. Parsons, *Neuroscience Lett.s,* **2001**, 306, 81-84.

[138] D. L. Flynn, D. P. Becker, D. P. Spangler, R. Nosal, G. W. Gullikson, C. Moummi, D.-C. Yang, *Bioorganic & Medicinal Chem. Lett.s,* **1992**, 2, 1613-1618.

[139] A. Baxter, J. Bent, K. Bowers, M. Braddock, S. Brough, M. Fagura, M. Lawson, T. McInally, M. Mortimore, M. Robertson, *Chemistry Lett.s,* **2003**, 13, 4047-4050.

[140] G. Zoidis, I. Papanastasiou, I. Dotsikas, A. Sandoval, R. G. Dos Santos, Z. Papadopoulou-Daifoti, A. Vamvakides, N. Kolocouris, R. Felix, *Bioorganic & Medicinal Chem.* **2005**, 13, 2791-2798.

[141] C. Shen, D. Bullens, A. Kasran, P. Maerten, L. Boon, J. M. F. G. Aerts, G. van Assche, K. Geboes, P. Rutgeerts, J. L. Ceuppens, *Int'l Immunopharmacology,* **2004**, 4, 939-951.

[142] S. Reissmann, F. Pineda, G. Vietinghoff, H. Werner, L. Gera, J. M. Stewart, I. Paegelow, *Peptides,* **2000**, 21, 527-533.

[143] W. J. Hoekstra, J. B. Press, M. P. Bonner, P. Andrade-Gordon, P. M. Keane, K. A. Durkin, D. C. Liotta, K. H. Mayo, *Bioorganic & Medicinal Chem. Lett.s,* **1994**, 4, 1361-1364.

[144] N. Tsuzuki, T. Hama, T. Hibi, R. Konishi, S. Futaki, K. Kitagawa, *Biochemical Pharmacology,* **1991**, 41, R5-R8.

[145] K. Kitagawa, N. Mizobuchi, T. Hama, T. Hibi, R. Konishi, S. Futaki, *Chem. & Pharmaceutical Bulletin (Tokyo),* **1997**, 45, 1782-1787.

[146] M. Manoharan, K. L. Tivel, P. D. Cook, *Tetrahedron Lett.s,* **1995**, 36, 3651-3654.

[147] N. Lomadze, H. J. Schneider, *Tetrahedron Lett.s,* **2002**, 43, 4403 - 4405.

[148] L. Moine, S. Cammas, C. Amiel, P. Guerin, B. Sebille, *Polymer,* **1997**, 38, 3121-3127.

[149] I. Habus, Q. Zhao, S. Agrawal. *Bioconjugate Chem.,* **1995**, 6, 327-331; See also: M. Manoharan, K. L. Tivel, P. D. Cook, *Tetrahedron Lett.s,* **1995**, *36*, 3651-3654.

[150] C. L. D. Gibb, X. Li, B. C. Gibb, **PNAS**, **2002**, 99(8), 4857-4862; See also: S. Aoki, M. Shiro, E. Kimura, *Chemistry - A European J.*, **2002,** 8(4), 929-939; See also: S. B. Copp, S. Subramanian, M. J. Zaworotko, *J. Amer. Chem. Soc.*, 1992, 114 (22), 8719-8720.

[151] D. Ranganathan, S. Kurur, *Tetrahedron Lett.s,* **1997**, 38, 1265-1268.

[152] A. K. Dillow, A. M. Lowman (Editors), *Biomimetic Materials & Design, Biointerfacial Strategies, Tissue Engineering, and Targeted Drug Delivery* Marcel Dekker, New York, NY, **2002**.

[153] K. Busch, R. Tampé, *Rev.s in Molecular Biotechnology* **2001**, 82, 3-24.

[154] J. H. Kim, J.-A. Hong, M. Yoon, M. Y. Yoon, H.-S. Jeong, H. J. Hwang, *J. Biotechnology,* **2002**, 96, 213 - 221.

[155] C. J. Noren, S. J. Anthony-Cahil, M. C. Griffith, P. G. Schultz, *Science*, **1989,** 244, 182-188.

[156] J. A. Piccirilli, T. Krauch, S. E. Moroney, S. A. Benner, *Nature*, **1990,** 343, 33-43.

[157] Annon., *Host-Guest Molecular Interactions, from Chemistry to Biology*, CIBA Foundation Symposia Series, No. 158, J. Wiley & Sons, New York, NY, **1991**.

[158] L. Mandolini, R. Ungaro (Editors), *Calixarenes in Action*, World Scientific Pub. Co., New York, NY, **2000**.

[159] D. Ranganathan, M. P. Samant, R. Nagaraj, E. Bikshapathy, *Tetrahedron Lett.s,* **2002**, 43, 5145-5147.

[160] D. Ranganathan, V. Haridas, I. L. Karle, *Tetrahedron,* **1999**, 55, 6643-6656.

[161] D. Ranganathan, A. Thomas, V. Haridas, S. Kurur, K. P. Madhusudanan, R. Roy, A. C. Kunwar, A. V. Sarma, M. Vairamani, K. D. Sarma, *J. Organic Chem.,* **1999**, 64, 3620-3629.

[162] D. Ranganathan, V. Haridas, S. Kurur, R. Nagaraj, E. Bikshapathy, A. C. Kunwar, A. V. Sarma, M. Vairamani, *J. Organic Chem.,* **2000**, 65, 365-374.

[163] D. Ranganathan, V. Haridas, R. Nagaraj, I.L. Karle, L. Isabella, *J. Organic Chem.,* **2000**, 65, 4415-4422.

[164] I. L. Karle, *J. Molecular Structure,* **1999**, 474, 103-112.

[165] I. L. Karle, D. Ranganathan, *J. Molecular Structure,* **2003**, 647, 85-96.

[166] C. Jaime, J. Redondo, F. Sanchez-Ferrando, A. Virgili, *J. Molecular Structure,* **1991**, 248, 317-329.

[167] K. Fujita, W-H. Chen, D.-Q. Yuan, Y. Nogami, T. Koga, *Tetrahedron, Asymmetry,* **1999**, 10, 1689–1696.

[168] D. Krois, U. H. Brinker, *J. Amer. Chem. Soc.*, **1998,** 120(45), 11627-11632.

[169] C. Karakasyan, M.-C. Millot, C. Vidal-Madjar, *J. Chromatography B,* **2004**, 808, 63-67.

[170] F. D. Ayres, S. I. Khan, O. L. Chapman, *Tetrahedron Lett.s,* **1994**, 35, 8561-8564.

[171] T. Ishizone, H. Tajima, S. Matsuoka, S. Nakahama, *Tetrahedron Lett.s,* **2001**, 42, 8645-8647.

Table I: Some physical properties of diamondoids mostly compiled by ChevronTexaco

www.moleculardiamond.com

Diamondoid Chemical Formula	**Molecular Structure**	**Mw**	**MP** [^{o}C]	**aBP** [^{o}C]	**ρ** [g/cc]	**Crystal Structures**
Adamantane $C_{10}H_{16}$		136.240	269.	135.5 @ 10 *mm Hg*	1.07	Cubic, fcc
Diamantane $C_{14}H_{20}$		188.314	236.5	272	1.21	Cubic, Pa_3
Triamantane $C_{18}H_{24}$	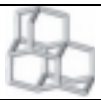	240.390	221.5	330	1.24	Orthorhombic, Fddd
Tetramantanes $C_{22}H_{28}$	 [1(2)3]	292.466	NA	NA	NA	NA
	 [121]		174	NA	1.27	Monoclinic, $P2_1/n$
	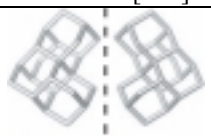 [123]		NA	NA	1.32	Triclinic, P1
Pentamantanes $C_{26}H_{32}$	 [1212]	344.543	NA	NA	1.26	Orthorhombic, $P2_12_12_1$
	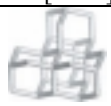 [12(3)4]		NA	NA	NA	Monoclinic, $P2_1/n$
	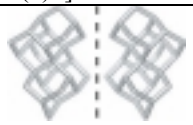 [1234]		NA	NA	1.30	NA
	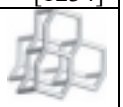 [1(2,3)4]		NA	NA	1.33	Orthorhombic, Pnma
	 [1213]		NA	NA	1.36	Triclinic, P-1
	 [12(1)3]		NA	NA	NA	NA
Cyclohexamantane (*peri-condensed*) $C_{26}H_{30}$	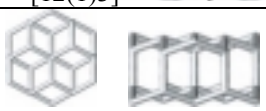 *Top* [12312] *Side*	342.528	>314	NA	1.38	Orthorhombic, Pnma
Heptamantanes $C_{30}H_{34}$	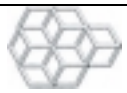 [121321]	394.602	NA	NA	1.35	Monoclinic, C2/m (#12)
	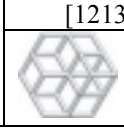 [123124]	394.602	NA	NA	NA	NA

aBP=apparent boiling point, MP=melting point, Mw=molecular weight, ρ =normal density

Table II: Vapor pressure equations of adamantane and diamantane for liquid-vapor and solid-vapor phase transitions

Diamondoid	**Phase Transition Kind**	***ln* P [kPa] =**	**Temp. Range [K]**	**Reference**
Adamantane	liquid-vapor	-4670 / T + 14.75	T > 543 K	[13]
	solid-vapor	- 6570/T + 18.18	483 - 543	[13]
		- 6324.7/T + 17.827	366 - 443	[16]
		- 9335.6/T + 65.206 - 15.349 *log* T	313 - 443	[16]
		- 7300/T + 31.583 - 4.376 *log* T	333 - 499	[17]
Diamantane	liquid-vapor	-5680/T + 14.858	516 - 716	[13]
	solid-vapor	-7330/T + 18.00	498 - 516	[13]
		-7632.5/T + 18.333	353 - 493	[17]
		-18981.3/T+190.735 -55.4418 *log* T	332 - 423	[17]

Table III: Thermodynamic properties of adamantane and diamantane. In this table the average of the values reported by various investigators are reported

PROPERTY	Diamondoid		Value	Units	T[K]	References
ΔH^{of}_{gas}	Adamantane		-133.6	kJ/gmol		[10,19-21]
	Diamantane		-145.9	kJ/gmol		[10]
ΔH^{of}_{solid}	Adamantane		-191.1	kJ/gmol		[10,19-22]
	Diamantane.		-241.9	kJ/gmol		[10]
S^{o}_{solid}	Adamantane. (crystalline phase II)		195.83	J/gmol•K		[23,24]
	Diamantane. (crystalline phase III)		200.16	J/gmol•K		[25]
C_P^{solid} (solid phase I)	Adamantane.		189.74	J/gmol•K	298.15	[23]
	Diamantane.		220.2	J/gmol•K	295.56	[26]
			223.22		298.15	[25]
$\Delta H^{o}_{sublimation}$	Adamantane.		59.9	kJ/gmol		[10,16,21,27,28]
	Diamantane.		96.	kJ/gmol	305.-333	[29]
$\Delta H_{phase.transition}$	Adam. (Solid I-Solid II)		3.376	kJ/gmol	208.62	[23,24]
	Diam.	Solid I-Solid III	4.445	kJ/gmol	407.22	[26]
		Solid I-Solid II	8.960	kJ/gmol	440.43	
		Solid I-–Liquid	8.646	kJ/gmol	517.92	
$\Delta S_{phase.transition}$	Adam. (Solid I-Solid II)		16.18	J/mol•K	208.62	[26]
	Diam.	Solid I-Solid III	10.92	J/mol•K	407.22	
		Solid I-Solid II	20.34	J/mol•K	440.43	
		Solid I-–Liquid	16.69	J/mol•K	517.92	
$\Delta H^{o}_{combustion}$	Adam. (solid phase)		-6030.04	kJ/gmol		[10,16,20,21]
	Diam. (solid phase)		-8125.58	kJ/gmol		[29]

Note: Solid adamantane possesses two crystalline phases and diamantane exists in three crystalline phases.

Table IV: Thermodynamic properties of methyl-derivatives of adamantane and diamantane. In this table the average of the values reported by various investigators are reported.

DIAMONDOID	ΔH^{of}_{gas} [kJ/gmol]	ΔH^{of}_{solid} [kJ/gmol]	$\Delta H^{o}_{sublimation}$ [kJ/gmol]	$\Delta H^{o}_{combustion}$ [kJ/gmol] (solid phase)	**References**
ADAMMANTANE	- 133.6	-191.1	59.9	- 6030.04	See Table II
1-METHYL ADAMANTANE	- 171.6	- 240.1	67.7	- 6661.1	[10,30]
1,3-DIMETHYL ADAMANTANE	-219.0	-287.3	67.8	-7294.0	[30]
1,3,5-TRIMETHYL ADAMANTANE	-255.0	-333.0	77.8	-7927.4	[30]
1,3,5,7-TETRAMETHYL ADAMANTANE	-283.3	- 370.7	82.4	- 8568.7	[10,30]
2-METHYL ADAMANTANE	-151.7	- 220.8	67.7	- 6680.4	[10,30]
DIAMANTANE	-145.9	-241.9	96.	- 8125.6	See Table II
1-METHYL DIAMANTANE	-166.7	-247.4	80.6	- 8799.4	[10]
3-METHYL DIAMANTANE	-157.3	-260.4	103.1	-8786.36	[10]
4-METHYL DIAMANTANE	-182.1	-261.5	79.4	-8786.2	[10]

Table V: Solubilities of Diamondoids in Liquid Solvents at 25^{O} C. From [13].

Solvent	Adamantane (wt%)	Diamantane (wt%)
Carbon tetrachloride	7.0	5.0
Pentane	11.6	4.0
Hexane	10.8	3.9
Heptane	10.4	3.7
Octane	10.0	3.9
Decane	8.9	3.5
Undecane	7.9	3.2
Tridecane	7.3	2.7
Tetradecane	7.5	2.3
Pentadecane	7.1	2.2
Cyclohexane	11.1	6.3
Benzene	10.9	4.3
Toluene	9.9	4.5
m-Xylene	9.8	4.5
p-Xylene	9.6	4.5
o-Xylene	9.6	4.1
THF	12.0	4.0
Diesel oil	7.5	2.7
1,3, Dimethyl-adamantane	6.0	2.0

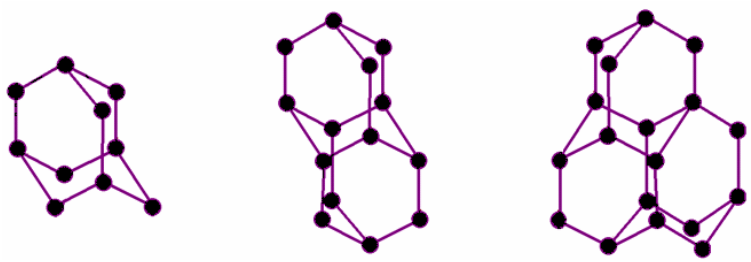

Figure 1: Molecular structures of adamantane, diamantane and trimantane, the smaller diamondoids, with chemical formulas $C_{10}H_{16}$, $C_{14}H_{20}$ and $C_{18}H_{24}$, respectively.

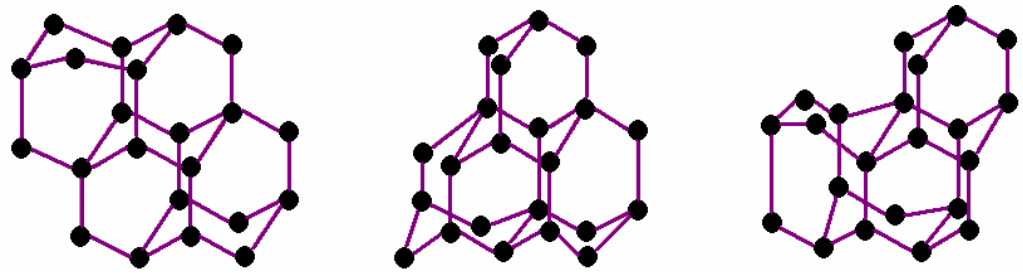

Figure 2: There are three possible tetramantanes all of which are isomeric, respectively from left to right as anti-, iso- and skew-tetramantane. Anti- and skew-tetramantanes, each, possess two quaternary carbon atoms, whereas iso-tetramantane has three quaternary carbon atoms. The number of diamondoid isomers increase appreciably after tetramantane.

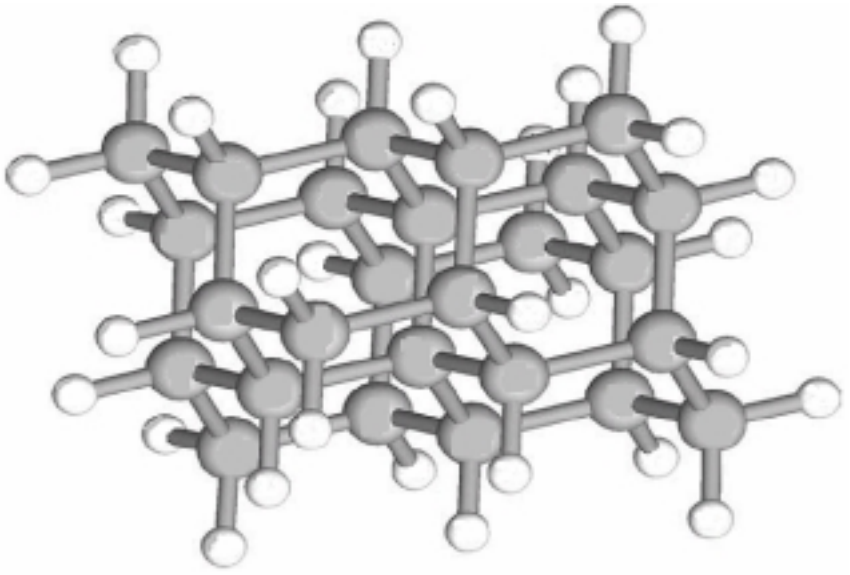

Figure 3: Molecular structure of (*peri-condensed*) cyclohexamantane ($C_{26}H_{30}$). Darker spheres represent carbon atoms while lighter spheres are hydrogen atoms.

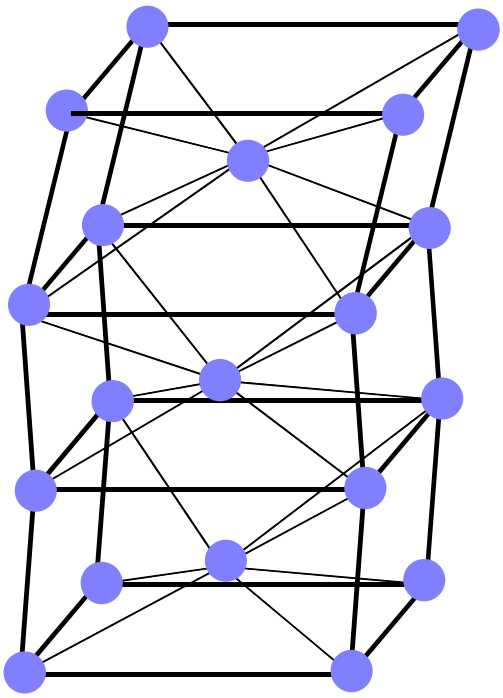

Figure 4: The quasi-cubic units of crystalline network for 1,3,5,7-tetrahydroxyadamantane. Molecules have been shown as blue spheres and hydrogen bonds as solid linking lines. This crystalline structure is similar to that of CsCl. From [8].

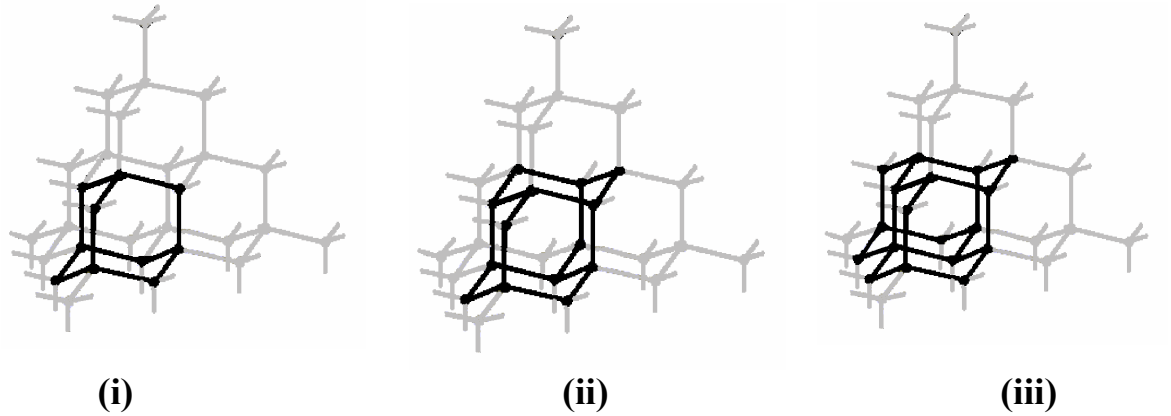

(i) **(ii)** **(iii)**

Figure 5: The relation between lattice diamond structure and (i). adamantane, (ii). diamantane and (iii), triamantane structures.

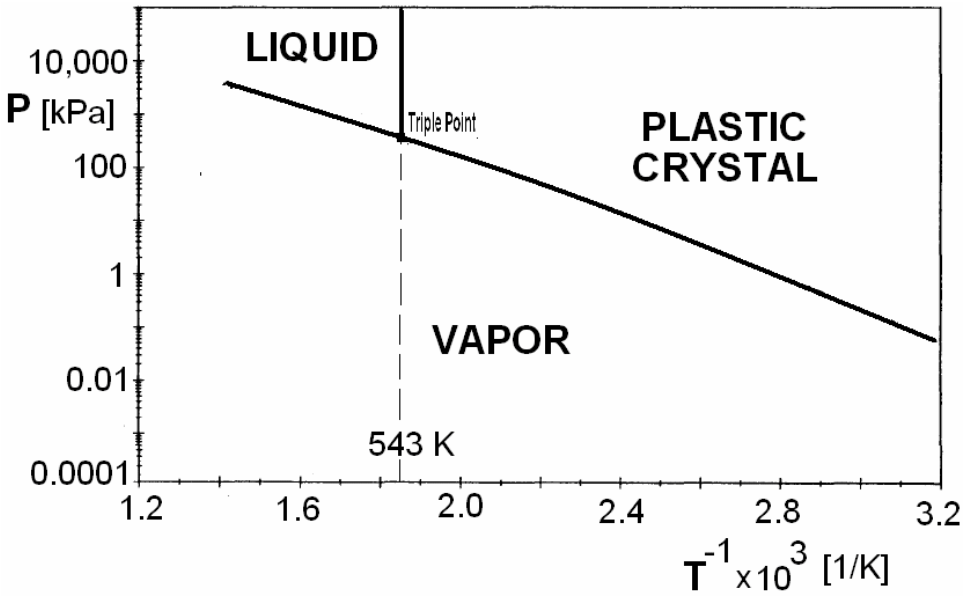

Figure 6: Vapor-Liquid-Solid (plastic crystal) phase diagram of adamantane. The phase transition from plastic crystal to rigid crystal phase occurs at 208.6 K (1/T=0.004794 K^{-1}). This diagram is based on the data of Table II.

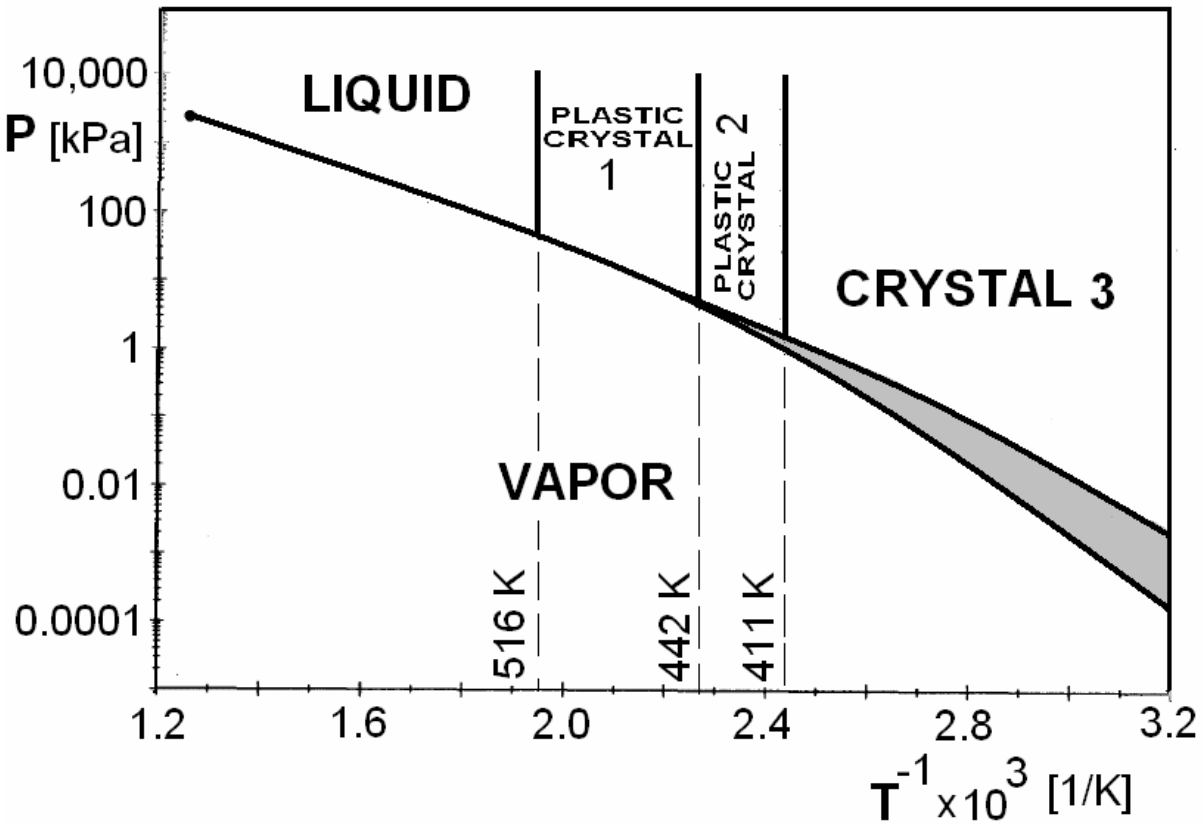

Figure 7: Vapor-Liquid-Solids (plastic crystal 2, plastic crystal 2, crystal 3) phase diagram of diamantane. This diagram is based on the data of Table II. The shaded area between vapor and plastic crystal 2 & crystal 3 phase transitions is indicative of the error range of the available data**.**

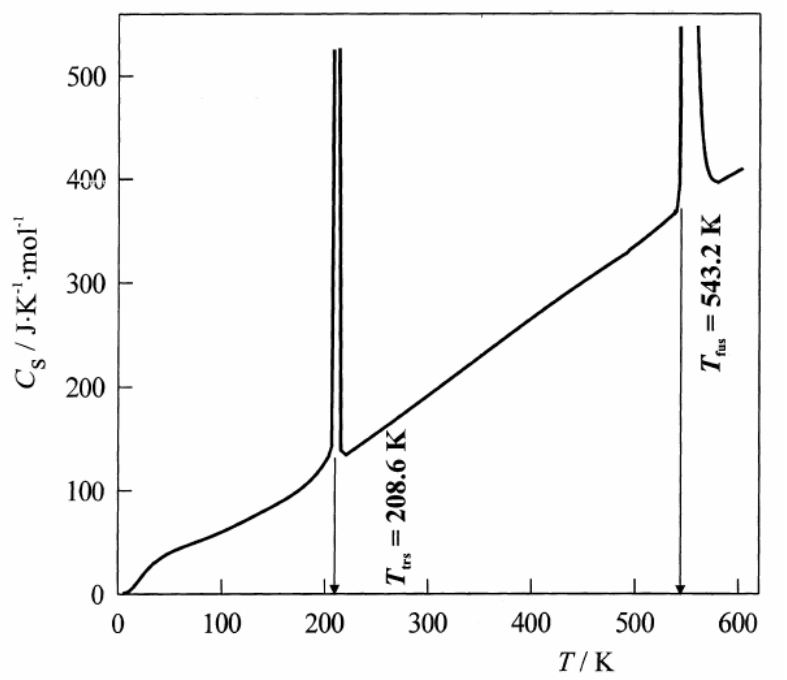

Figure 8: The temperature dependence of the heat capacity in the condensed state for adamantane [5] as measured by a scanning calorimeter. T_{trs} stands for temperature of transition from rigid crystal (fcc)-to-plastic crystal (cubic) state of adamantane and T_{fus} stands for fusion temperature.

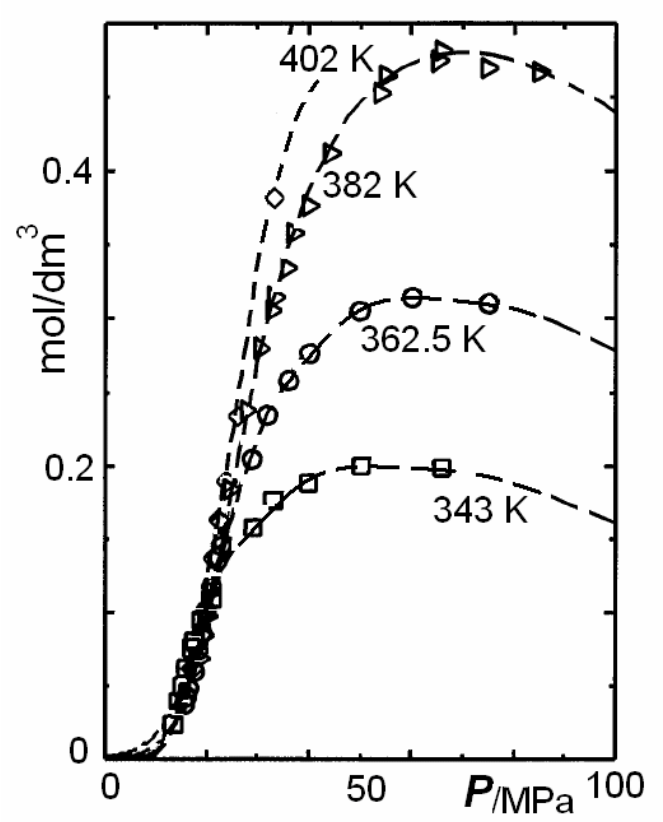

Figure 9: Effect of temperature and pressure on solubility (in units of mol/dm^3) of adamantane in dense (supercritical) carbon dioxide gas. Data from [36].

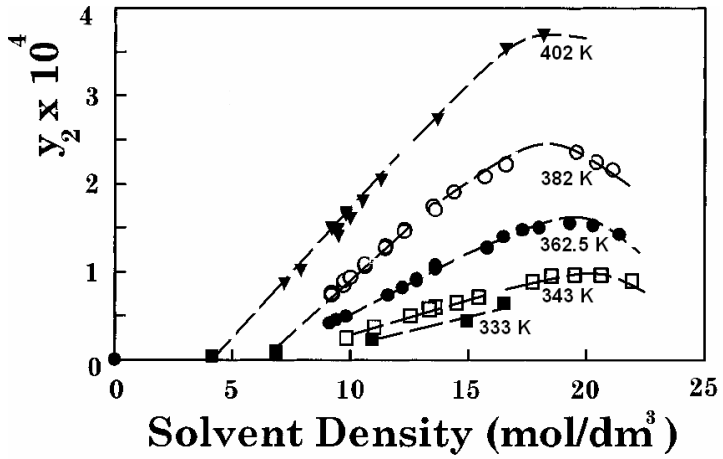

Figure 10: Effect of temperature and supercritical solvent density on solubility of adamantane (in units of mole fraction) in dense (supercritical) carbon dioxide. Data of isotherm at 333 K is from [35]. Data of isotherms at 343 K, 362.5 K, 382 K and402 K are from [37].

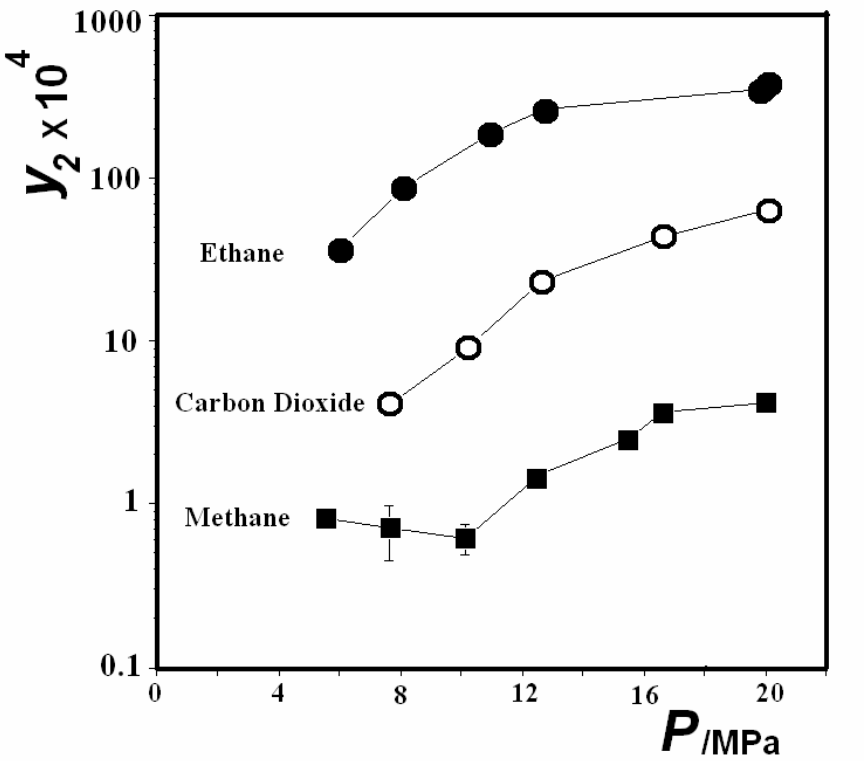

Figure 11: Effect of pressure on the solubility (in units of mole fraction) of adamantane in dense (supercritical) carbon dioxide, methane, and ethane gases at 333 K. Data from [35].

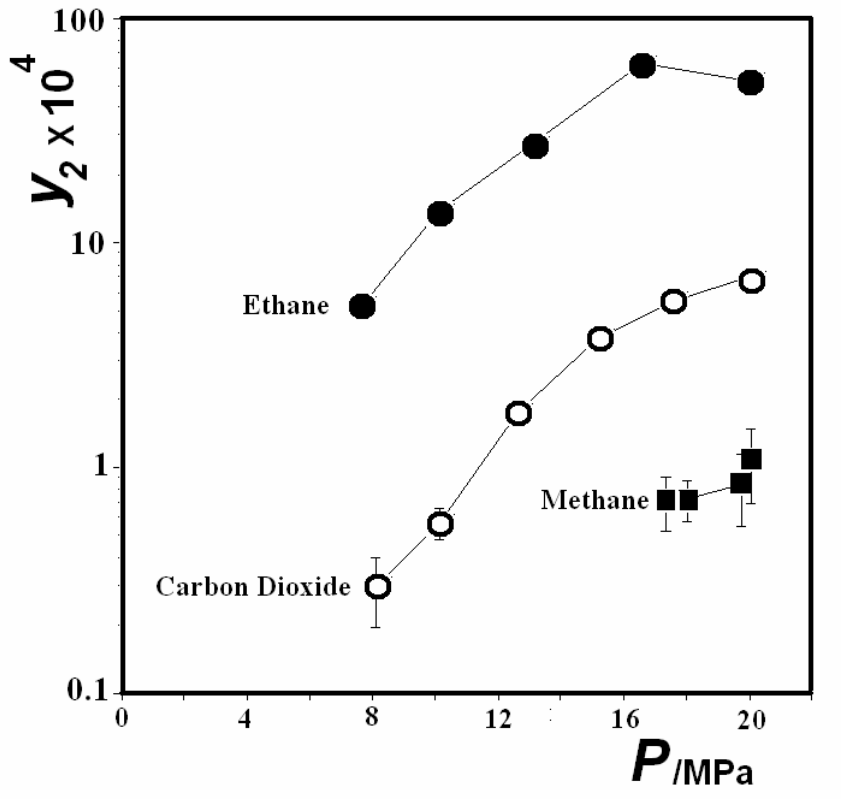

Figure 12: Effect of pressure on solubility (in units of mole fraction) of diamantane in dense (supercritical) gases at 333 K (for carbon dioxide and ethane) and at 353 K (for methane) – Data from [35].

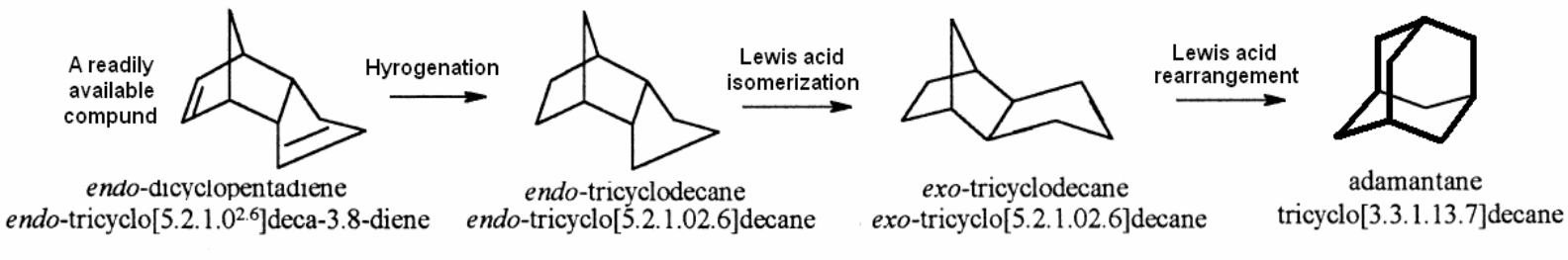

Figure 13: Various stages in synthesis of adamantane based on the work reported in [43,44].

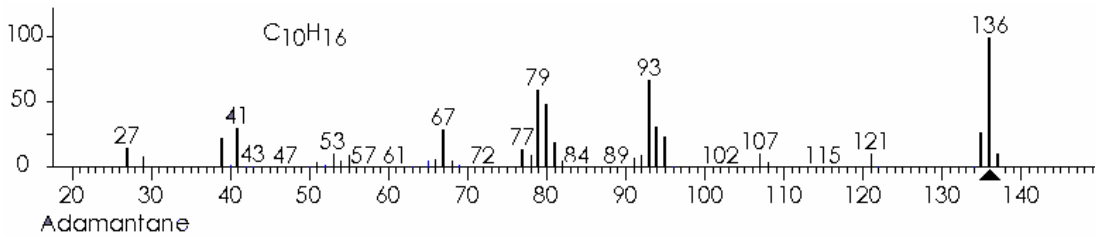

Figure 14: Standard molecular fragmentation spectrum of adamantane (136 m/z)

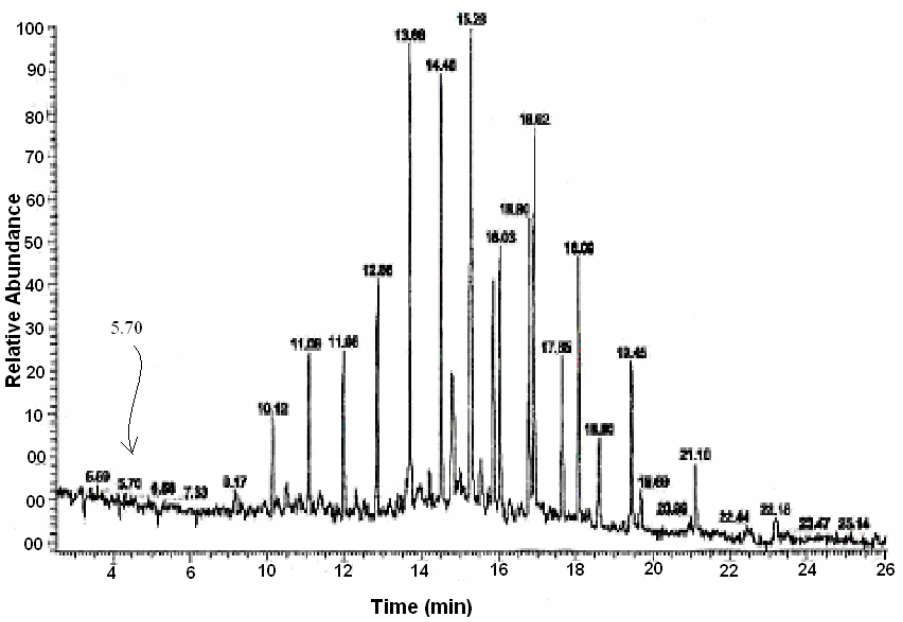

Figure 15: Gas chromatogram of a gas condensate (NGL=natural-gas liquid) sample [74]. The peak with retention time of 5.70 eluted between nC_{15} and nC_{16} is indicative of the probable existence of diamantane in the sample.

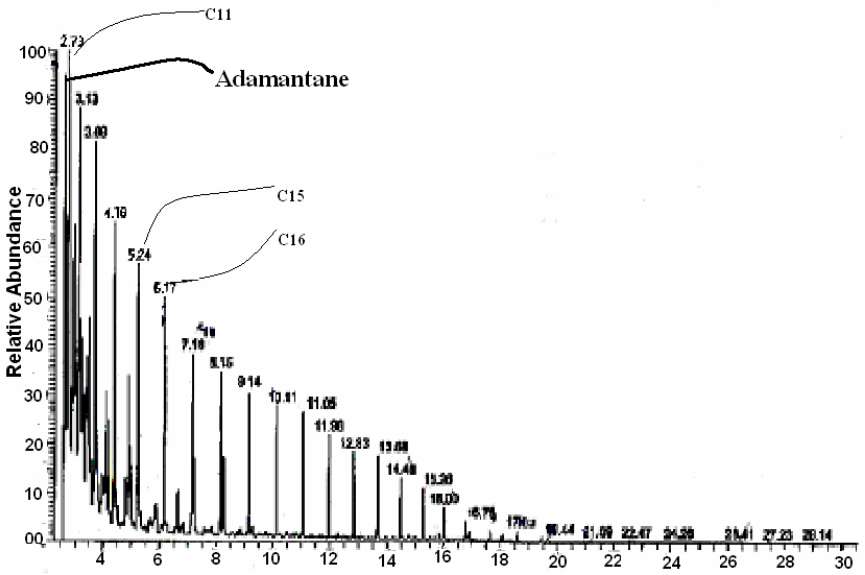

Figure 16 – Gas chromatogram of a crude oil sample showing the possible existence of adamantane and diamantane in the sample.

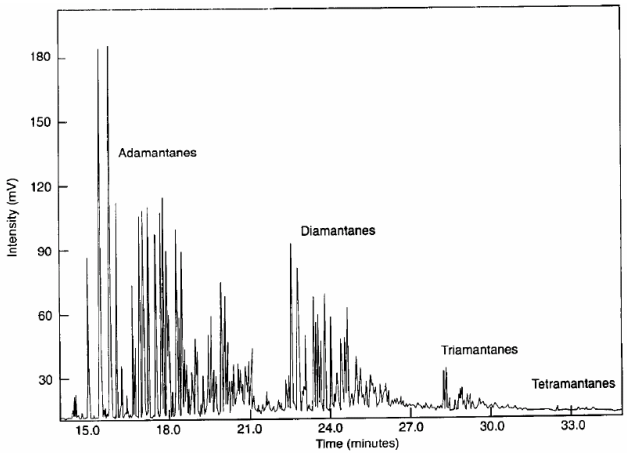

Figure 17: Gas chromatogram of a diamondoid-rich gas-condensate (NGL) sample showing clusters of peaks representing adamantanes, diamantanes, triamantanes and tetramantanes. From: [11].

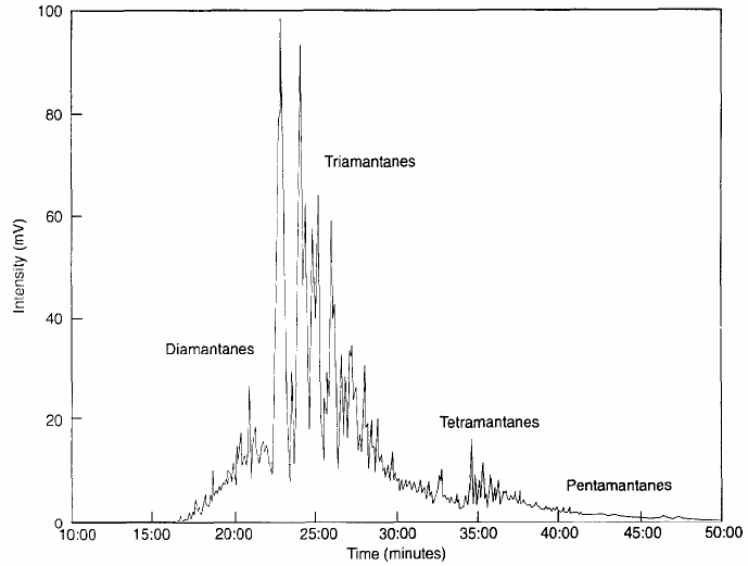

Figure 18: Gas chromatogram from the full-scan CC/MS analysis of a high-temperature distillation fraction (343" C^{+}) containing diamondoids. From: [11].

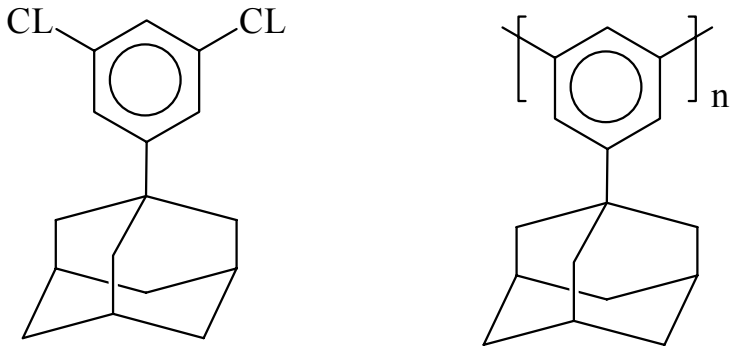

Figure 19: (Left) 1,3-dichloro-5-(1-admantyl) benzene monomer and (Right) adamantly-substituted poly(m-phenylene) which is shown to have a high degree of polymerization and stability decomposing at high temperatures of around 350 °C. From [89].

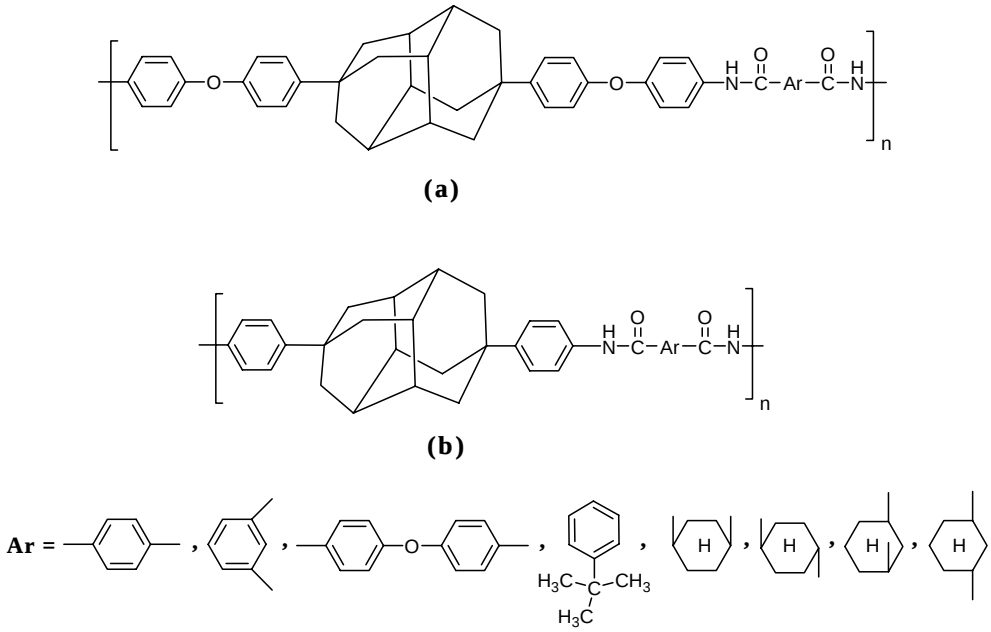

Figure 20: Diamantane-based polyamides; (a) derived from 4,9-bis[4-(4-aminophenoxy)phenyl]diamantane and (b) derived from 4,9-bis(4-aminophenyl)diamantane. From [90].

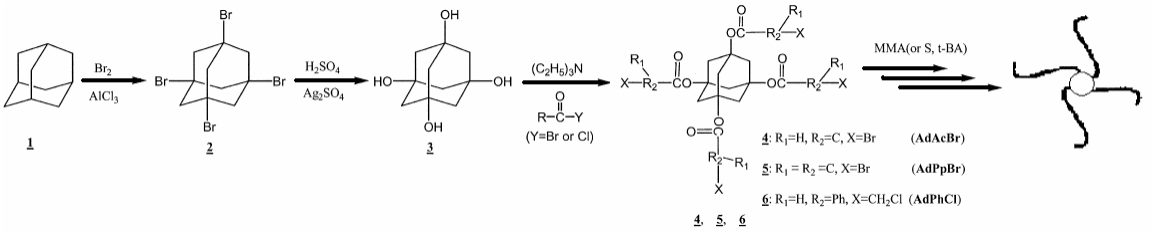

Figure 21: Atom transfer radical polymerization (ATRP) synthetic route to tetrafunctional initiators of a star polymer with adamantly (adamantane core). From [91].

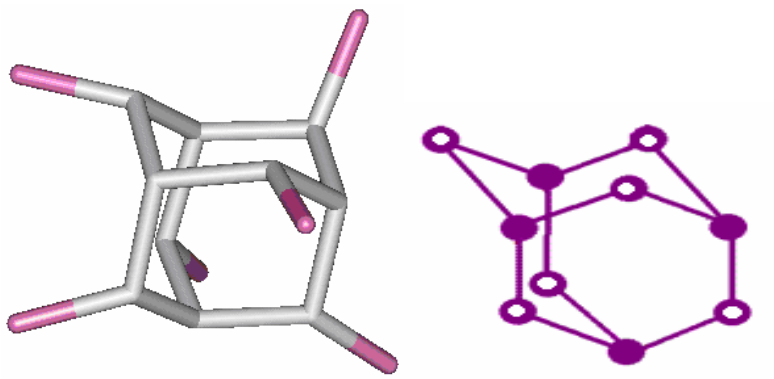

Figure 22: Demonstration of the six linking groups of adamantane.

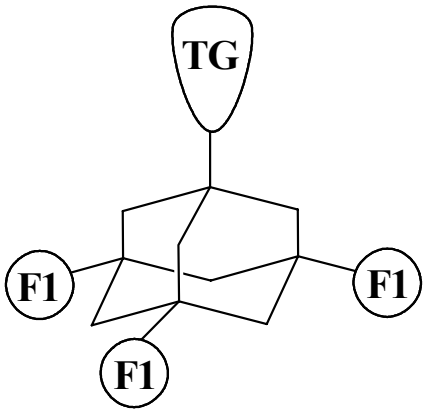

Figure 23: Schematic drawing which shows adamantane as a molecular probe with three fluorophore groups (F1) and a targeting part (TG) for specific molecular recognition. From [112].

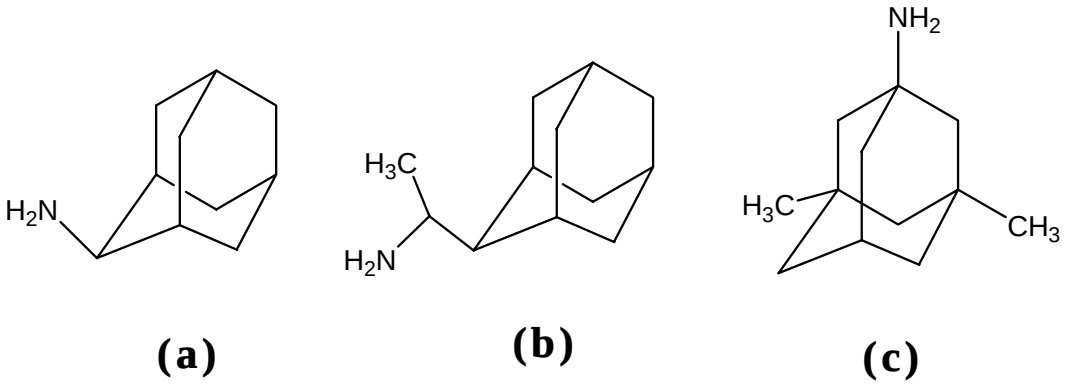

Figure 24: Chemical structures of (a) Amantadine. (b) Rimantadine. (c) Memantine.

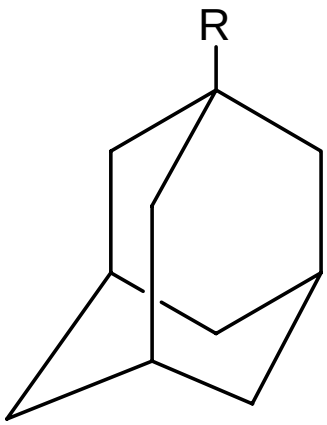

(I) R = NH_2-Tyr-(D-Ala)-Gly-Phe-Leu-CO-O-
(II)R = NH_2-Tyr-(D-Ala)-Gly-Phe-Leu-CO-NH-

Figure 25: The adamantane-conjugated [D-Ala2]Leu-enkephalin prodrugs. From [144].

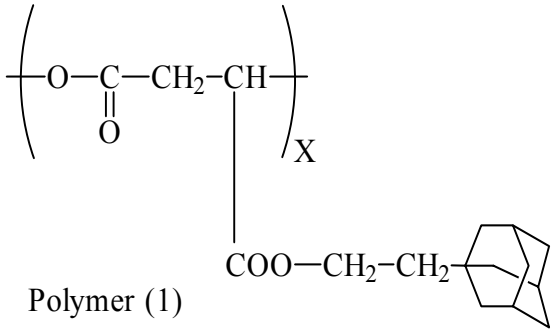

Polymer (1)

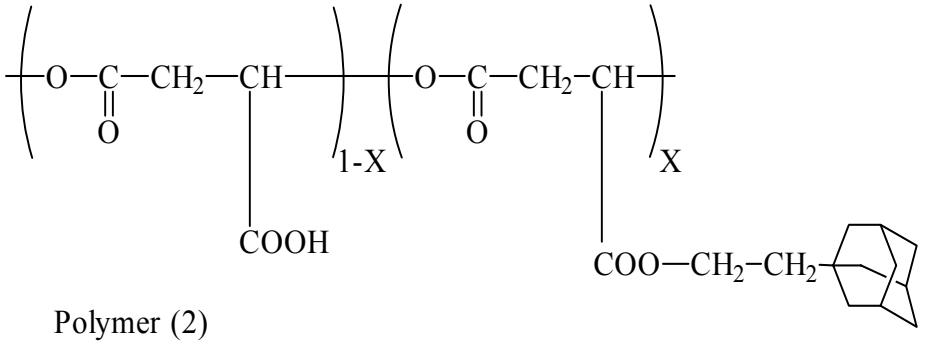

Polymer (2)

Figure 26: Polymer (1) {poly (ethyladamantyl β-malate)} is hydrophobic and polymer (2) {poly(β-malic acid-co-ethyladamantyl β-malate} is hydrophilic. Both of these plymers are used as carriers for different drugs [148].

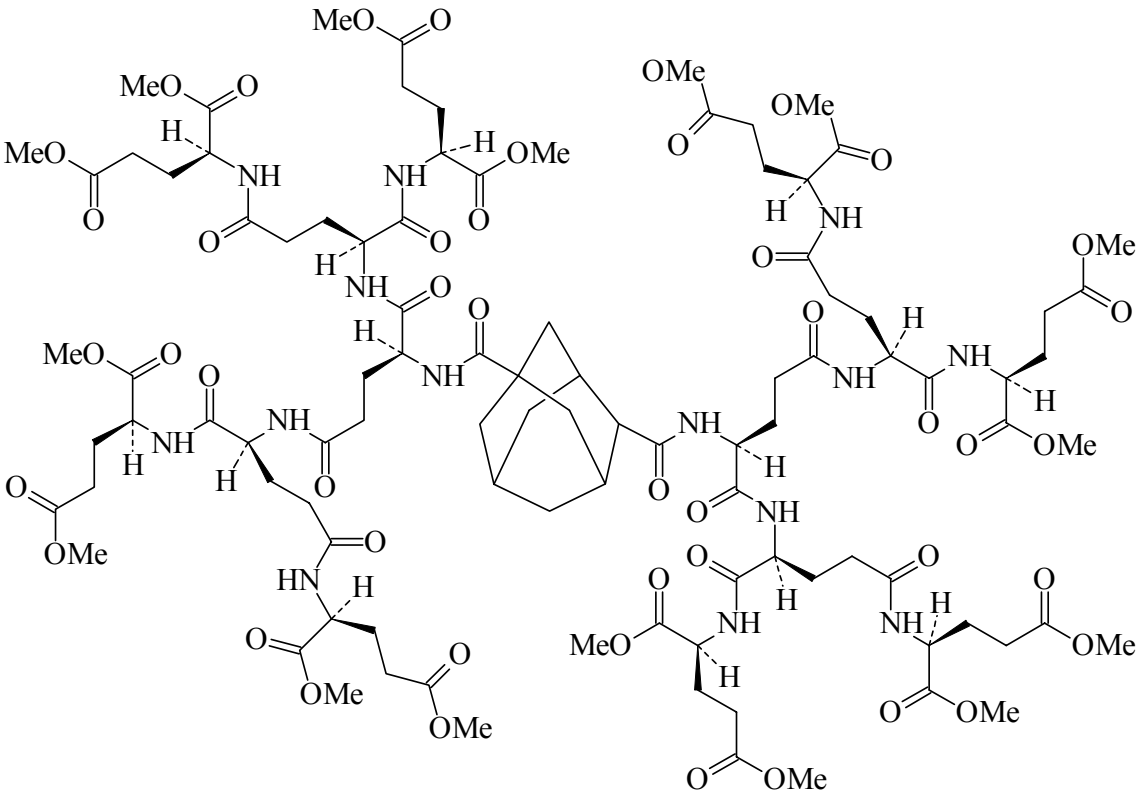

Figure 27: Adamantane nucleus with amino acid substituents creates a peptidic matrix [151]. The represented structure is Glu4-Glu2-Glu-[ADM]-Glu-Glu2-Glu4.

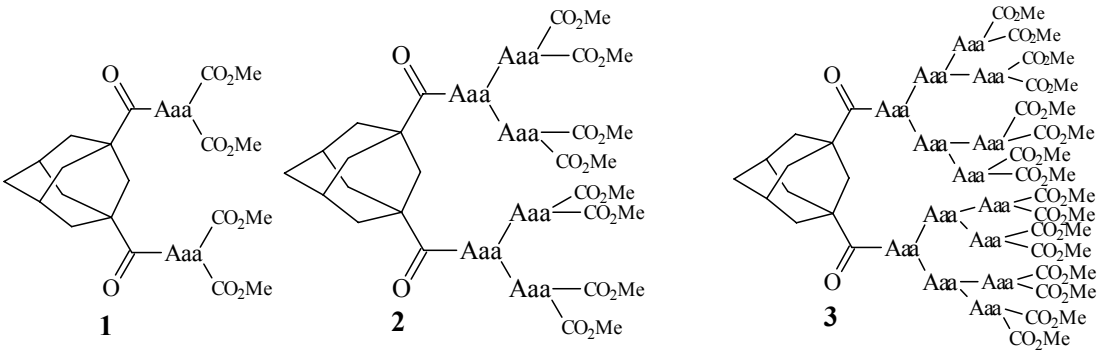

Figure 28: A dendrimer-based approach for the design of globular protein mimic using glutamic (Glu) and aspartic (Asp) acids as the building blocks and adamantyl as the core [151].

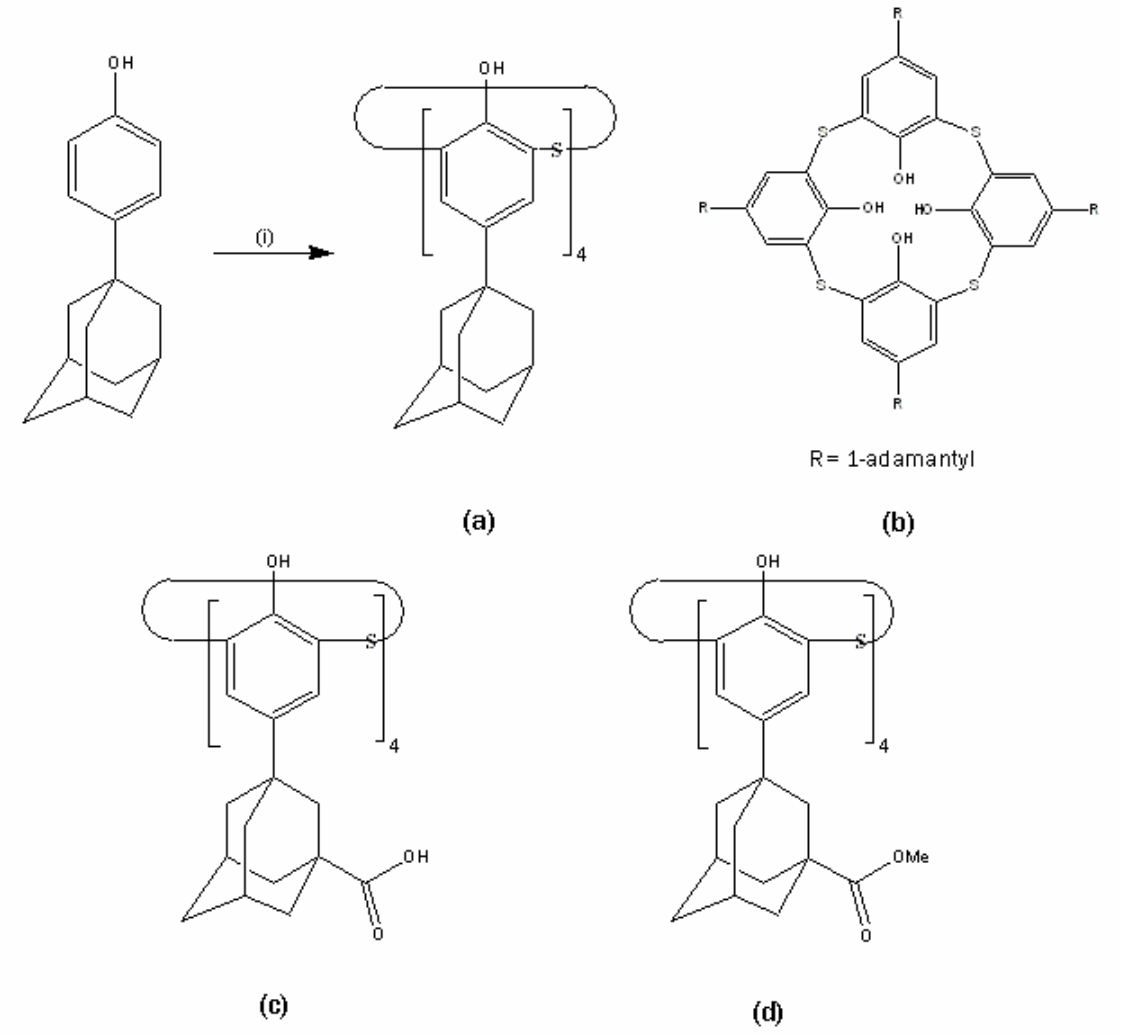

Figure 29: a) Synthesis route of the molecule (b): (i) S8, NaOH, tetraethyleneglycol dimethyl ether, heat, (28%). b) Adamantane Upper rim derivative based on the thiacalix[4]arene platform. c,d) The carboxylic acid and ester derivative of adamantane can be also used as substituents. From [109].

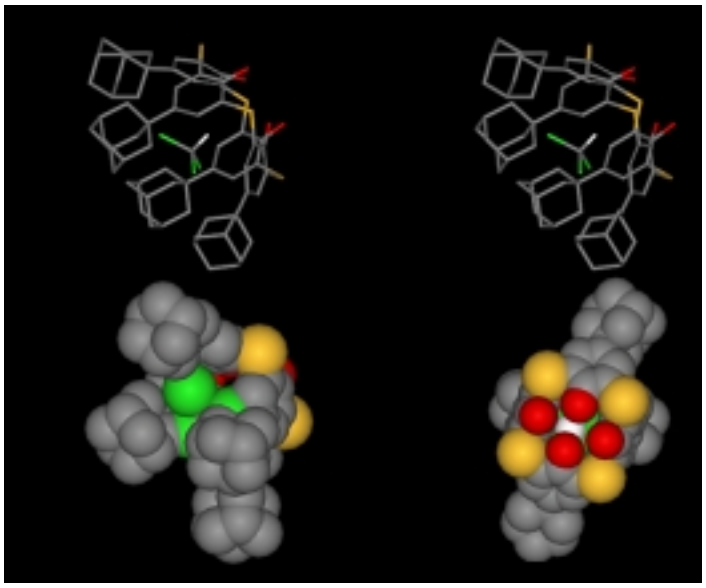

Figure 30: Lateral stereo views of adamantane-derivative thiacalix[4]arene (top) presented in Figure 29. A $CHCl_3$ molecule has been entrapped inside the inclusion compound. The bottom view (left bottom) and top view (right bottom) have been also shown. H atoms have been removed from the inclusion compound for more clarity. (Cl, OH, S, H and C atoms have been colored green, red, yellow, white and gray, respectively).

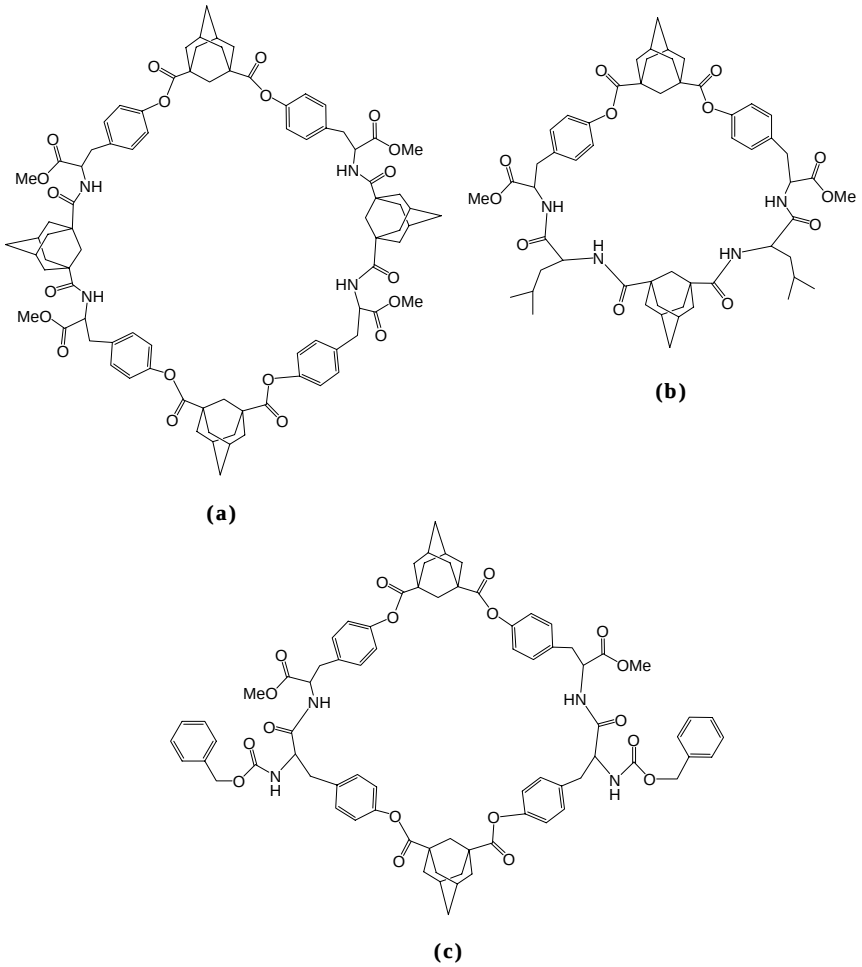

Figure 31: Adamantane-bridged tyrosine-based cyclodepsipeptides are suitable models for host-guest studies and they are also able to act as ion transporters. From [161].

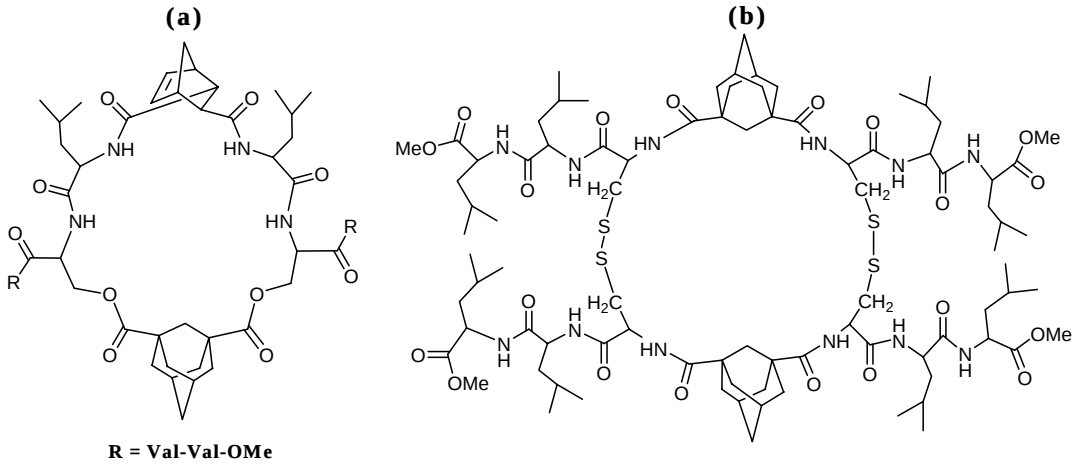

Figure 32: Adamantane-containing norbornene ( )-constrained cyclic peptides possess the ability to transport ions across the model membranes in both specific and non-specific ways [162].

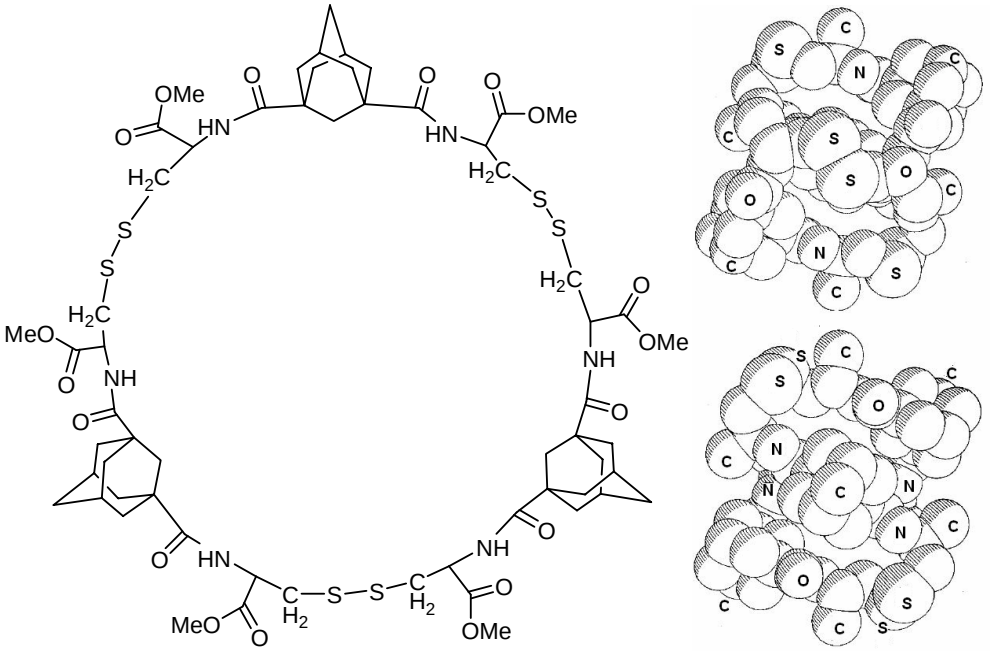

Figure 33: The cyclo (Adm-Cyst)3 as adopts a figure-eight like helical structure. The chiral amino acid, cystine, configuration determines the helix disposition (right-handed or left handed helix). Adamantane plays an important role as a ring size controlling agent. From [163].

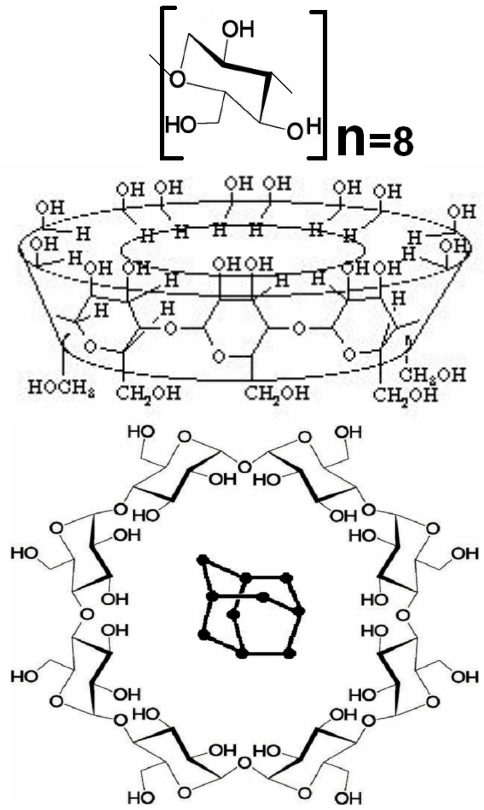

Figure 34: Chemical formula of γ cyclodextrin consisting of eight glucose molecules with adamantane as is the guest entrapped within its hydrophobic cavity. Structures of α and β cyclodextrins will be similar but made up of six and seven (n=6, 7) glucoses, respectively

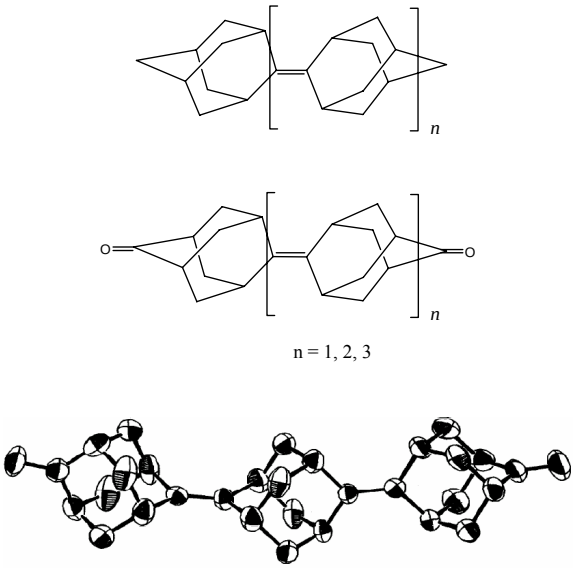

Figure 35: Poly-adamantane molecular rods. From [170].

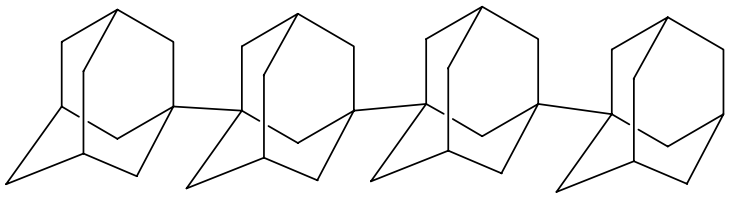

Figure 36: Synthetic design of a molecular rod made of adamantanes: The tetrameric 1,3-adamantane. From [171].